Acta Cryst. (1979). B**35**, 934–945

Charge Density in Parabanic Acid from X-ray and Neutron Diffraction

BY B. M. CRAVEN

Department of Crystallography, University of Pittsburgh, Pittsburgh, Pennsylvania 15260, *USA*

AND R. K. MCMULLAN

Chemistry Department, Brookhaven National Laboratory, Upton, New York 11973, *USA*

(*Received* 30 *August* 1978; *accepted* 3 *January* 1979)

Abstract

Parabanic acid (imidazoletrione, $C_3H_2N_2O_3$) at room temperature, is monoclinic, space group $P2_1/n$ with a = 10·690 (2), b = 8·194 (1), c = 5·049 (1) Å, β = 92·74 (6)° and has four molecules per unit cell. The nuclear configuration has been determined from 1245 neutron intensities (sin $\theta/\lambda < 0{\cdot}76$ Å^{-1}, $\lambda = 1{\cdot}0470$ Å) to give e.s.d.'s in bond lengths and angles of 0·002 Å and 0·2° or less. The X-ray (Mo $K\alpha$) intensity data (2149 reflections with $F_o > 3\sigma$; sin $\theta/\lambda < 1{\cdot}0$ Å^{-1}) were used to determine the electronic charge density by a least-squares procedure based on a pseudoatom model with a multipole expansion at the octapole level. In various refinements, different parameter groups including third-order temperature factors were assumed to have fixed neutron values. Asphericity shifts (0·01 Å) of the O atoms are attributed to deformations of the pseudoatom core density. Unsuccessful efforts were made to determine the extent to which thermal motion and/or core polarization might be responsible for these shifts. Each kind of pseudoatom in the molecule (C,N,O,H) is found to have a characteristic asphericity in the valence-shell charge density. The CN and CO bonds appear to be polar. There is no obvious effect of the molecular interactions on the valence-shell density. However, O core polarizations may be involved in the unusually short (2·77 Å) C···O interactions.

Introduction

The crystal structure of parabanic acid (Davies & Blum, 1955) has been redetermined by neutron and X-ray diffraction in order to study the electronic charge-density distribution. Parabanic acid was chosen because the molecule (Fig. 1) may be regarded as a simple analog of the polar ring portion of the drug-active barbiturates. Parabanic acid is unlikely to act directly as a drug, because of the ease with which it is hydrolyzed to form oxaluric acid (Andrews & Sell, 1955; Shieh & Voet, 1975). However, the chemical relationship between parabanic acid and the barbiturates is expected to give rise to similarities in their electronic structures, and hence in the nature of their molecular interactions. Both form hydrogen-bonded crystal complexes with adenine derivatives (Shieh & Voet, 1975; Voet, 1972) and with urea (Colman & Medlin, 1970; Gartland & Craven, 1974). Both molecules form unusually short C···O interactions involving the carbonyl groups. The crystal structure of parabanic acid (Fig. 2) provides the shortest known intermolecular C···O distance (2·77 Å). These interactions have been discussed by Bolton (1964) and by Bürgi, Dunitz & Shefter (1974). The experimentally determined charge densities in parabanic acid and polymorph II of barbital (5,5-diethylbarbituric acid) are compared elsewhere (Fox, Weber & Craven, 1979).

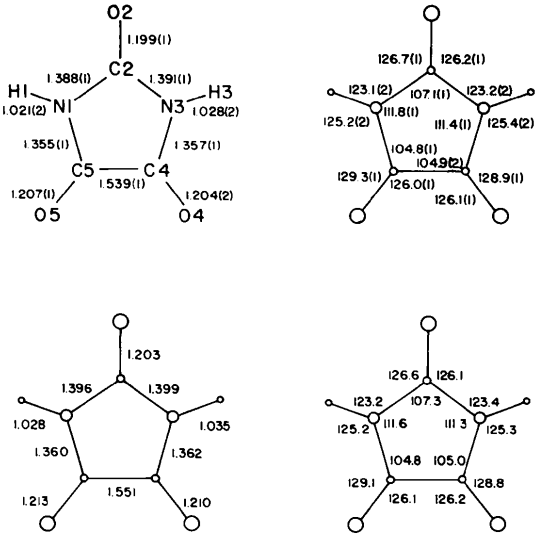

Fig. 1. Parabanic acid. Atomic nomenclature, bond lengths (Å) and angles (°). The top figures show the observed neutron values. The bottom figures are the values corrected for rigid-body librations.

0567-7408/79/040934-12$01.00

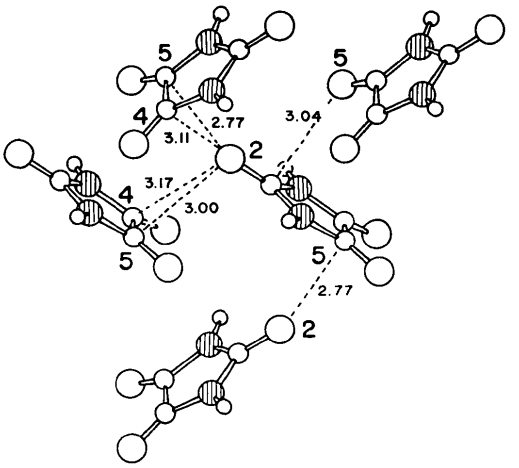

Fig. 2. The partial crystal structure of parabanic acid. Spheres of diminishing size represent O, N, C, H atoms, with N atoms cross-hatched. The crystal *c* axis runs from left to right, with the *b* axis almost in the plane of the page. Short intermolecular C···O distances are in Å. The layer of molecules shown here is hydrogen bonded to others in front and behind.

Room-temperature diffraction data were collected because a low-temperature X-ray facility was not available at the beginning of the study. This imposed limitations on the analysis, but they were not severe since parabanic acid melts with decomposition at 517 K, and at room temperature the thermal parameters are smaller than in most organic structures.

The neutron structure determination

Parabanic acid was obtained as monoclinic prisms with the forms {100}, {010} and {101} by slow evaporation of an acetone solution at room temperature. Small single crystals suitable for X-ray study were readily formed, but all the larger crystals (2 mm) were twinned on (001).

A single crystal suitable for neutron data collection was separated from its twin by cleavage and fracture. The selected fragment extinguished sharply under a polarizing microscope and showed no evidence of twinning in X-ray precession photographs. The crystal shape and dimensions were determined with a microscope and indices were assigned to three natural and three fracture planes. The volume of the polyhedron was found to be 1·78 mm^3. The neutron diffraction data were collected at the Brookhaven High Flux Beam Reactor with a monochromatized beam obtained by reflection from the (002) planes of beryllium. The neutron wavelength of 1·0470 (2) Å was determined by least-squares fit of $\sin^2\theta$ data for a standard KBr crystal (a_0 = 6·5964 Å). The parabanic acid crystal was aligned with its c^* axis along the φ axis of the diffractometer. The lattice parameters (Table 1) were determined by a least-squares fit to $\sin^2\theta$ data of 18 reflections ($46 < 2\theta < 62°$). Intensity data in one independent quadrant were collected by an $\omega/2\theta$ step-scan method to a limiting $\sin\theta/\lambda$ of 0·76 Å^{-1}. Scans of 3·0° in 2θ were used within a limiting $\sin\theta/\lambda$ of 0·40 Å^{-1}, and scans of variable lengths, computed from the formula $\Delta(2\theta) = (1·29 + 3·00\tan\theta)°$, were used beyond this value. The two reflections that were monitored periodically showed no significant variation of intensity with time. The backgrounds were evaluated from counts summed at the scan extremes, taking 20% of the total number of points sampled. The variance of an intensity was assumed to be $\sigma^2(I) = I + 5B + (0·02I)^2$, where I is the integrated intensity and B is the total background. The data were corrected for absorption (μ = 0·0748 mm^{-1}) assuming the mass-absorption coefficient for hydrogen (2390 mm^2 g^{-1}) which was determined experimentally for the crystal structure of barbital (McMullan, Fox & Craven, 1978). The maximum and minimum correction factors for F_o^2 were 1·111 and 1·060 respectively. The agreement on averaging symmetry-related reflections of the *hk*0 zone was 1·8%.

Refinement by full-matrix least-squares methods was begun with the atomic parameters given by Davies & Blum (1955). The function $\sum w(F_o^2 - F_c^2)^2$ was minimized for the 1245 recorded reflections, including 59 that had small but not significantly negative F_o^2 values. The neutron-scattering lengths ($\times 10^{-11}$ mm) used were: −0·374 for H, 0·6648 for C, 0·5803 for O, and 0·940 for N. The scale factor and isotropic extinction parameter (Coppens & Hamilton, 1970) were first adjusted in three cycles of refinement; the 90 atomic parameters were then included, and the refinement continued until convergence was achieved with all parameter changes less than 0·2σ. The final $R(F^2)$ and $R_w(F^2)$ were 0·036 and 0·043, respectively, and the final quadratic mean error (QME)† was 1·16. A plot of $(w|F_o^2 - F_c^2|)$ *vs* F_o^2

† Refinement criteria are given by $R(F) = \sum_H \Delta_H / \sum_H |F_o|_H$; $R_w(F) = (\sum_H w_H \Delta_H^2 / \sum_H w_H |F_o|_H^2)^{1/2}$ and QME $= [\sum_H w_H \Delta_H^2/(n_o - n_{param})]^{1/2}$ where $\Delta_H = |F_o|_H - |F_c|_H$. Corresponding expressions for $R(F^2)$ *etc.* are obtained by substituting F^2 for $|F|$.

Table 1. *Crystal data for parabanic acid*

Monoclinic, $P2_1/n$; Z = 4($C_3H_2N_2O_3$) per cell, m.p. 517 K (decomp.).

	X-ray	Neutron	X-ray*
a	10·690 (2) Å	10·692 (4) Å	10·685 (1) Å
b	8·194 (1)	8·194 (3)	8·194 (1)
c	5·049 (1)	5·051 (2)	5·054 (1)
β	92·74 (6)°	92·74 (2)°	92·73 (3)°

* Values determined by Davies & Blum (1955).

Table 2. *Atomic parameters and their e.s.d.'s*

(*a*) Positional parameters

The fractional coordinates and their e.s.d.'s ($\times 10^5$) determined from the neutron data are given above values from the X-ray data.

	x	y	z
N(1)	19405 (4)	32759 (7)	46571 (12)
	19373 (7)	37253 (11)	46575 (19)
C(2)	29853 (7)	36849 (9)	32702 (15)
	29851 (7)	36857 (10)	32678 (18)
O(2)	30035 (10)	45138 (13)	13149 (22)
	30037 (12)	45111 (16)	12948 (27)
N(3)	40130 (5)	29451 (7)	45650 (12)
	40161 (7)	29455 (12)	45604 (20)
C(4)	36711 (6)	20821 (9)	67074 (15)
	36683 (6)	20824 (9)	67074 (17)
O(4)	43171 (8)	13037 (14)	82635 (23)
	43170 (8)	13024 (16)	82896 (27)
C(5)	22432 (6)	23076 (9)	67670 (14)
	22424 (5)	23052 (9)	67677 (16)
O(5)	15727 (8)	17329 (13)	83832 (19)
	15720 (8)	17209 (14)	83947 (22)
H(1)	10573 (16)	36585 (25)	41090 (41)
H(3)	49105 (14)	30512 (26)	39425 (39)

(*b*) Anisotropic temperature factors

The values of $U_{ij} \times 10^4$ Å^2 were obtained for the temperature factor in the form $T = \exp(-2\pi^2 \sum_i \sum_j h_i h_j a_i^* a_j^* U_{ij})$. The neutron values are given first. The X-ray values given underneath are from the refinement in which the variables included the positional parameters for non-hydrogen atoms.

	U_{11}	U_{22}	U_{33}	U_{12}	U_{13}	U_{23}
N(1)	192 (2)	282 (3)	300 (3)	40 (2)	−6 (2)	24 (2)
	166 (2)	265 (3)	269 (4)	44 (2)	−10 (2)	21 (3)
C(2)	255 (3)	238 (3)	237 (4)	6 (2)	12 (3)	26 (3)
	249 (3)	231 (3)	215 (3)	5 (2)	11 (2)	35 (3)
O(2)	472 (6)	359 (5)	316 (5)	3 (4)	18 (4)	116 (4)
	441 (5)	328 (5)	278 (5)	3 (4)	19 (4)	111 (4)
N(3)	187 (2)	356 (3)	336 (3)	1 (2)	60 (2)	85 (3)
	167 (3)	339 (4)	294 (4)	11 (3)	64 (3)	83 (4)
C(4)	137 (3)	295 (3)	281 (4)	4 (2)	10 (2)	59 (3)
	127 (2)	287 (3)	250 (3)	8 (2)	5 (2)	63 (3)
O(4)	193 (4)	470 (6)	444 (6)	−2 (4)	−51 (4)	194 (5)
	173 (3)	437 (5)	396 (5)	−3 (3)	−48 (3)	173 (5)
C(5)	144 (3)	268 (3)	227 (3)	5 (2)	24 (2)	−2 (3)
	134 (2)	248 (3)	207 (3)	4 (2)	26 (2)	−5 (3)
O(5)	200 (3)	420 (5)	305 (5)	−13 (3)	83 (3)	35 (4)
	180 (3)	383 (4)	270 (4)	−6 (3)	74 (3)	30 (4)
H(7)	289 (7)	553 (11)	523 (10)	126 (7)	−20 (7)	51 (9)
H(3)	288 (7)	566 (11)	514 (10)	−18 (7)	128 (7)	104 (9)

(*c*) Pseudoatom radial parameters

These are values of (a.u., bohr^{-1}) for the charge density radial functions of the Slater type. Values given first are from the refinement with neutron values for all the atom positions. Values below were obtained when non-hydrogen positional parameters were included as variables.

C	N	O	H
3·25 (2)	3·89 (2)	4·40 (1)	2·14 (6)
3·30 (2)	3·93 (2)	4·38 (1)	2·06 (5)

(*d*) Population parameters

These values ($\times 10^2$) are for the angular charge-density functions referred to the crystal axes a, b, c^*. Paired values correspond to the respective radial parameters in (*b*).

	p_v	d_1	d_2	d_3
N(1)	499 (8)	4 (4)	−7 (3)	−1 (4)
	489 (8)	32 (7)	5 (6)	1 (7)
C(2)	406 (6)	0 (4)	42 (4)	29 (5)
	391 (6)	1 (6)	23 (7)	5 (9)
O(2)	600 (3)	6 (3)	11 (3)	−33 (4)
	614 (4)	0 (8)	16 (9)	41 (11)
N(3)	497 (7)	−11 (4)	−8 (3)	−1 (4)
	485 (8)	43 (7)	11 (6)	16 (7)
C(4)	411 (5)	14 (4)	−15 (4)	22 (5)
	398 (5)	22 (7)	−11 (7)	15 (8)
O(4)	596 (3)	15 (3)	−12 (3)	33 (4)
	607 (4)	16 (7)	1 (9)	48 (9)
C(5)	411 (5)	−27 (4)	−11 (4)	35 (4)
	398 (5)	−6 (6)	4 (6)	18 (8)
O(5)	595 (3)	25 (3)	20 (3)	26 (3)
	610 (4)	8 (6)	45 (8)	−19 (8)
H(1)	94 (6)	60 (10)	−36 (7)	46 (7)
	105 (6)	86 (12)	40 (7)	55 (7)
H(3)	91 (6)	−81 (11)	−10 (6)	18 (7)
	103 (6)	118 (13)	11 (6)	24 (7)

Table 2 (*cont.*)

	q_1	q_2	q_3	q_4	q_5
N(1)	13 (7)	−32 (15)	47 (16)	−9 (18)	−3 (5)
	12 (7)	−34 (14)	43 (15)	7 (18)	−7 (6)
C(2)	13 (8)	2 (15)	32 (16)	−269 (19)	21 (5)
	19 (8)	−3 (15)	−29 (16)	203 (19)	19 (5)
O(2)	61 (11)	−39 (22)	−38 (23)	9 (24)	−32 (7)
	53 (10)	41 (21)	33 (22)	26 (25)	−19 (7)
N(3)	2 (8)	−32 (16)	−31 (16)	1 (19)	4 (5)
	1 (7)	32 (15)	27 (15)	18 (20)	3 (5)
C(4)	54 (7)	−149 (14)	103 (14)	−206 (18)	2 (5)
	54 (6)	110 (14)	63 (15)	−174 (19)	3 (4)
O(4)	15 (9)	43 (19)	61 (18)	83 (24)	3 (7)
	10 (8)	34 (18)	−53 (18)	64 (24)	10 (6)
C(5)	62 (7)	76 (13)	152 (14)	156 (18)	7 (4)
	48 (6)	37 (13)	75 (15)	−140 (18)	2 (4)
O(5)	3 (8)	−125 (16)	131 (16)	−22 (22)	16 (6)
	−3 (8)	94 (16)	93 (17)	−66 (21)	−9 (5)
H(1)	47 (11)	8 (19)	81 (21)	−15 (21)	31 (6)
	68 (13)	20 (19)	99 (22)	27 (21)	−40 (6)
H(3)	61 (12)	−23 (18)	−152 (24)	58 (19)	2 (5)
	90 (14)	26 (18)	191 (25)	56 (19)	−13 (6)

	o_1	o_2	o_3	o_4	o_5	o_6	o_7
N(1)	20 (6)	49 (6)	−153 (16)	30 (32)	22 (5)	18 (5)	24 (4)
	23 (5)	50 (5)	−151 (16)	22 (30)	24 (5)	13 (4)	19 (4)
C(2)	38 (7)	48 (7)	239 (22)	102 (40)	0 (7)	25 (6)	−32 (5)
	37 (7)	40 (7)	192 (21)	77 (39)	3 (6)	16 (6)	−34 (5)
O(2)	19 (6)	1 (6)	21 (16)	104 (34)	−2 (5)	17 (5)	−13 (4)
	21 (5)	4 (5)	13 (15)	103 (32)	3 (5)	10 (5)	9 (4)
N(3)	43 (6)	38 (6)	144 (17)	85 (34)	26 (5)	−10 (5)	38 (4)
	45 (6)	32 (6)	−124 (16)	96 (32)	30 (5)	6 (5)	35 (4)
C(4)	80 (7)	3 (7)	91 (19)	271 (39)	55 (6)	5 (6)	−10 (5)
	79 (7)	12 (6)	60 (18)	238 (39)	59 (6)	0 (6)	4 (5)
O(4)	−14 (5)	1 (5)	19 (16)	24 (31)	5 (4)	−22 (5)	6 (4)
	15 (5)	−2 (5)	47 (15)	55 (30)	7 (4)	−27 (5)	2 (4)
C(5)	39 (7)	−70 (7)	145 (19)	263 (30)	73 (6)	20 (6)	−11 (5)
	55 (6)	59 (6)	101 (19)	228 (38)	−66 (6)	20 (6)	0 (4)
O(5)	11 (5)	24 (5)	36 (14)	34 (28)	9 (4)	−8 (5)	−2 (4)
	11 (5)	27 (5)	20 (14)	11 (27)	5 (4)	−1 (4)	−1 (3)

(*e*) Population parameters in the double dipole refinement

Dipole population parameters ($\times 10^2$) are for the angular charge-density functions referred to the crystal axes, a, b, c^*. Values for the 'diffuse' dipole with radial parameter $\alpha = 4{\cdot}35$ (1) a.u. are given above values for the 'sharp' dipole with $\alpha = 8$ (2) a.u.

	d_1	d_2	d_3
O(2)	0 (7)	9 (7)	26 (11)
	3 (4)	−6 (5)	37 (6)
O(4)	6 (6)	16 (8)	−42 (13)
	1 (4)	13 (5)	52 (7)
O(5)	−10 (6)	30 (10)	−16 (9)
	5 (3)	−35 (5)	24 (5)

showed the weighting used in the analysis to be appropriate.

The neutron data were found to be extensively affected by extinction. The smallest extinction factors ($0{\cdot}38 \times F_c^2$) were obtained for reflections 200 and 020. It thus became important to determine the extent that the assumed model for extinction might affect the atomic positional and thermal parameters. Nine least-squares refinements were carried out to test various extinction models proposed by Becker & Coppens (1974). Smaller values of $R(F^2)$, $R_w(F^2)$ and QME were obtained by assuming type I (mosaicity dominated) rather than type II (particle-size dominated) extinction. When a generalized model was assumed (particle-size dominating at low Bragg angle), values of the extinction parameters oscillated rather than converged. Better fits to the data were also obtained by assuming a Lorentzian rather than a Gaussian distribution of mosaicity. There was no significant improvement by assuming an anisotropic

rather than an isotropic model. The best description of extinction in this crystal, according to the Becker & Coppens formalism, was taken to be an isotropic model of type I with Lorentzian mosaicity, which gave $R(F^2)$ = 0·036, $R_w(F^2)$ = 0·043 and a QME of 1·17. The final neutron atomic parameters in Table 2 are from this refinement. However, it should be noted that there were no significant differences between these values and those obtained in the initial refinement with the Coppens & Hamilton (1970) model for extinction. Furthermore, there were no significant differences in nuclear positional parameters as a result of changing the extinction model, although there were changes in anisotropic thermal parameters. It is of interest that a type II model for extinction gave thermal parameters about 10% lower than the type I values, and in good agreement with the X-ray thermal parameters. However, the type II model gave a poor fit to the neutron data with $R(F^2)$ = 0·060, $R_w(F^2)$ = 0·074 and a QME of 2·00.

In the course of the X-ray structure determination, residual electron density maps indicated that the usual anisotropic or second-order temperature factors (U_{ij}) were inadequate for the O atoms. Accordingly, further refinements were carried out with the neutron data, including third-order temperature factors (Johnson, 1970). The revised model for thermal motion used ten additional parameters (c_{jkl}) per atomic nucleus, as defined by a Gram–Charlier expression (equation 5.2.3.9; Johnson & Levy, 1974). All nuclear positional and U_{ij} parameters changed by less than 1·0σ from the values previously obtained (Table 2). Values of 18 of the c_{jkl} parameters were possibly significant ($\geq 2\sigma$) of which the largest were 3·0σ and 3·3σ for two different O atoms.*

The R-factor ratio test (Hamilton, 1974) gave 96% probability that the additional 100 thermal parameters provided no improvement in the structure model. However, a further test was made to determine whether only certain atoms, such as the peripheral O or H atoms,

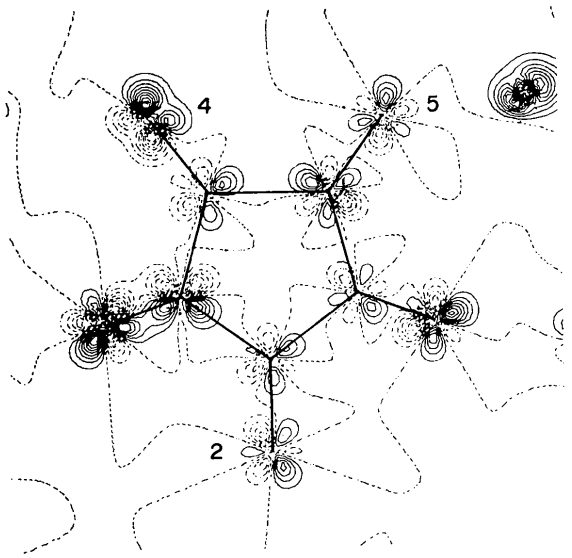

Fig. 3. Deformation map showing the antisymmetric component of the thermally averaged neutron-scattering density at each nucleus. The e.s.d. in the scattering density is near the second contour level.

* Lists of neutron and X-ray structure factors, c_{jkl} values and anisotropic thermal parameters have been deposited with the British Library Lending Division as Supplementary Publication No. SUP 34145 (40 pp.). Copies may be obtained through The Executive Secretary, International Union of Crystallography, 5 Abbey Square, Chester CH1 2HU, England.

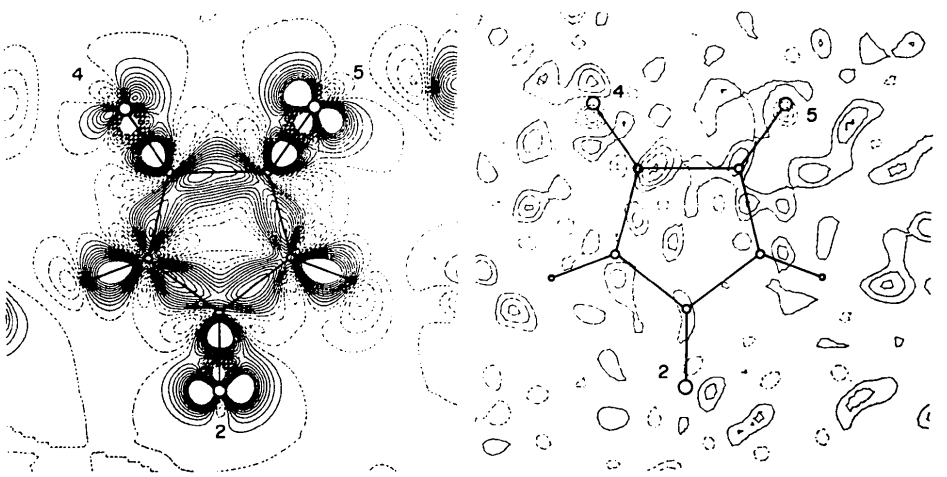

(a) (b)

Fig. 4. Maps for the X-ray refinement based on neutron positional parameters. (*a*) The map of deformations in the valence charge for the molecule at rest. Contours are at 0·05 e Å^{-3} up to a maximum of 0·5 e Å^{-3}. E.s.d.'s are 0·15 e Å^{-3} at about 0·3 Å from the O atom centers, and are from 0·03 to 0·07 e Å^{-3} in the bonding regions. (*b*) Difference Fourier synthesis showing the residual charge density. Contours are at 0·05 e Å^{-3} with the −1, 0, +1 contours omitted. The e.s.d. in the residual density is about 0·05 e Å^{-3}.

might require third-order temperature factors. As an alternative to seeking a graphical representation of the c_{jkl} factors (Johnson, 1970), deformations of the neutron-scattering density about each nucleus were modeled in terms of a multipole expansion with dipole, quadrupole and octapole terms, using the computer program which was developed for the X-ray structure refinement (see below). Population parameters for the deformations and a common radial parameter of $\alpha =$ 7 (1) a.u.* were determined by a least-squares method and used to obtain a deformation map (Fig. 3). This map is similar in some respects to the X-ray residual density map (Fig. 4*b*), *e.g.* at O(4). It was concluded that the effects of non-rectilinear nuclear vibrations were no more than marginally significant, but still merited some consideration in the X-ray structure determination.

The X-ray structure determination

(*a*) *Experimental*

The X-ray data were measured using an Enraf–Nonius CAD-4 computer-controlled diffractometer with graphite-monochromated Mo $K\alpha$ radiation. The unit-cell parameters and intensity data for reflections with $(\sin\theta/\lambda)_{max} = 1{\cdot}0$ Å^{-1} were obtained using a crystal 0·56 × 0·36 × 0·26 mm which was mounted with the c axis (the longest dimension) along the diffractometer φ axis. The unit-cell parameters (Table 1) were obtained by a least-squares fit of $\sin^2\theta$ values for 14 reflections with $29 < \theta < 35°$. Each reflection was measured at $+\theta$ and $-\theta$. The wavelength λ(Mo $K\alpha_1$) = 0·70926 Å was assumed.

Integrated intensities were measured by $\omega/2\theta$ scans with a scan width of $\Delta(2\theta) = (3{\cdot}2 + 1{\cdot}8\tan\theta)°$. Tests were made with film at the detector window to ensure that the virtual X-ray source and the diffracted beam were not partially obscured by so-called collimators. Intensities were collected for 4512 reflections of which 3783 were not symmetry related. The maximum time taken for each reflection was 2 min. The R factor for agreement between symmetry-related reflections was 0·011. The variance of an integrated intensity (I) was assumed to be $\sigma^2(I) = \sigma^2 + (0{\cdot}02I)^2$ where σ^2 is the variance based on counting statistics.

In azimuthal scans for several strong reflections at small Bragg angles, there were variations in integrated intensity which were considerably greater than could be attributed to simple X-ray absorption, *e.g.* 021 varied by 10%. This showed that extinction might be significant. All the intensity data were corrected for absorption ($\mu = 0{\cdot}169$ mm^{-1}), although the transmission factors were within a narrow range (0·95 ± 0·01). The expected severe extinction became apparent early in the least-squares refinement of the structure. Thus the correction factor for 021 was 0·58.

The effects of extinction on the X-ray structure determination were greatly reduced by collecting additional intensity data with a second crystal. This crystal was a small fragment (0·20 × 0·12 × 0·08 mm) cut from a crystal which was grown by rapid cooling of an acetone solution. The crystal was mounted with its longest dimension, c, along the diffractometer φ axis, and 1636 intensities with $(\sin\theta/\lambda)_{max} < 0{\cdot}7$ Å^{-1} were measured by $\omega/2\theta$ scans. The maximum time spent on each reflection was 4 min. The 71 reflections with calculated extinction factors less than 0·98 were deleted from the first crystal data set and the remainder were combined with the complete second data set using a least-squares scaling procedure (Hamilton, Rollett & Sparks, 1965). The data then consisted of 2149 non-symmetry-related reflections with $F > 3\sigma(F)$ and 1423 reflections with $F \le 3\sigma(F)$. Only the former were used for the structure refinement. They included 1067 reflections with $0{\cdot}7 < \sin\theta/\lambda < 1{\cdot}0$ Å^{-1}.

(*b*) *Method of analysis*

The structure refinement was based on Stewart's (1976) rigid pseudoatom model. The valence-shell electron density for each pseudoatom was represented by a multipole expansion as far as quadrupole terms for the H and octapole terms for the non-hydrogen pseudoatoms. Thus, the pseudoatom X-ray scattering factors in parabanic acid had the general form

$$\begin{aligned} f = f_{core} &+ p_v f_v + if_d(d_1 s_x + d_2 s_y + d_3 s_z) \\ &+ i^2 f_q[q_1(s_x^2 - s_y^2) + q_2 s_x s_y + q_3 s_x s_z + q_4 s_y s_z \\ &+ q_5(3s_z^2 - 1)] + i^3 f_o[o_1(s_x^2 - 3s_y^2)\, s_x \\ &+ o_2(3s_x^2 - s_y^2)\, s_y + o_3(s_x^2 - s_y^2)\, s_z + o_4 s_x s_y s_z \\ &+ o_5(5s_z^2 - 1)\, s_x + o_6(5s_z^2 - 1)\, s_y \\ &+ o_7(5s_z^2 - 3)\, s_z], \end{aligned}$$

where $i = \sqrt{-1}$ and (s_x, s_y, s_z) are the direction cosines of the Bragg vector with respect to a Cartesian axial system which was defined as a, b, c^*. The 16 refinable parameters p_v, d_i, q_i, o_i are the electron population parameters for monopole, dipole, quadrupole and octapole terms, respectively. The multipole angular scattering factors are similar to those defined by Stewart (1976) and used by Cromer, Larson & Stewart (1976). The spherical K-shell scattering factors (f_{core}) for non-hydrogen atoms are based on self-consistent field wavefunctions (Clementi, 1965). Anomalous core scattering was found to be negligible. The multipole one-electron radial scattering factors were assumed to correspond to crystal-space radial functions of the Slater type, $[4\pi(n + 2)!]^{-1}\alpha^{n+3} r^n \exp(-\alpha r)$. The explicit functions used in this structure determination were $f_v = (1 + c^2)^{-2}$ for

* In atomic units (bohr^{-1}). 1 bohr = 0·52918 Å.

H ($n = 0$); $f_v = (1 - c^2)(1 + c^2)^{-4}$ for non-hydrogens ($n = 2$); $f_d = (5c/3)(1 - c^2/5)(1 + c^2)^{-4}$; $f_q = 2c^2(1 + c^2)^{-4}$; $f_o = (16c^3/5)(1 + c^2)^{-5}$ (see equation A2 in Epstein & Stewart, 1977). The variable $c = (4\pi a_o/\alpha)(\sin\theta/\lambda)$ where $a_o = 1$ bohr = 0·52918 Å, θ is the Bragg angle, λ is the X-ray wavelength (Å) and α (in atomic units, bohr^{-1}) is a radial parameter which takes larger values as the pseudoatom becomes contracted in crystal space. The values of α for C, N, O and H pseudoatoms were refined by a least-squares procedure. A series of computer programs were written for pseudoatom least-squares refinement and the subsequent mapping of charge densities (Craven & Weber, 1977). The full-matrix least-squares refinement minimized the function $\sum w\Delta^2$ where $\Delta = |F_o| - |F_c|$ and $w = 1/\sigma^2(F_o)$.

(c) *X-ray refinement based on nuclear positions*

All atomic positional parameters and the H atom thermal parameters were fixed at the neutron values. The variables consisted of a scale factor, a parameter for type I isotropic extinction with Lorentzian crystal mosaicity, the non-hydrogen atom thermal parameters, and the pseudoatom parameters, giving a total of 199. Convergence was obtained with $R(F) = 0{\cdot}031$, $R_w(F) = 0{\cdot}018$ and QME of 1·31. The sum of the monopole population parameters, which gives the total valence charge on the molecule, was 41·9 (2) electrons, in excellent agreement with the value (42) for an electrically neutral molecule. For convenience, this sum was constrained to be 42, thus eliminating the scale factor for the structure factors as an independent variable. The refinement was completed in this way with no significant changes in the refinement criteria or the remaining structure parameters. The correlation factors were largest (0·9) between radial parameters (α) and corresponding monopole population parameters (p_v) and between certain temperature parameters (U_{ij}) and quadrupole population parameters (q_i) for the same atom.

The X-ray values of the temperature factors U_{ii} were systematically and significantly smaller than the neutron values. Similar results were obtained for putrescine diphosphate at 85 K (Takusagawa & Koetzle, 1979), but in some instances such differences are found to have the opposite sense, as in sulfamic acid at 78 K (Bats, Coppens & Koetzle, 1977) and melamine (Varghese, O'Connell & Maslen, 1977). In part, the differences for parabanic acid may come from the choice of a model to describe the neutron extinction, as described above. However, we have no satisfactory explanation for these effects.

The parameter values from this first refinement (Table 2) were used to calculate the maps in Figs. 4 and 5. The residual density map (Fig. 4*b*) is a ΔF Fourier synthesis using the 2149 reflections from the least-squares refinement. Only the largest differences from zero charge density (0·25 e Å^{-3}) are significant in terms of the e.s.d. in the observed density (0·05 e Å^{-3}). Thus, the density calculated from the rigid pseudoatoms, each convoluted with anharmonic thermal motion, appears to provide a good fit to the observed charge density at most points in the unit cell. The other maps (Figs. 4*a*, 5) show the electronic charge density derived from the multipole expression for a structure of static pseudoatoms. The density at each map point is the sum of terms from all pseudoatoms which have nuclei within 2·5 Å of that point.

In calculating these maps, it is assumed that the anisotropic temperature factors U_{ij} provide a correct description of the thermal motion of the pseudoatoms, and that the U_{ij} values are free from systematic error (Hirshfeld, 1977; Coppens & Stevens, 1977). These assumptions have not been justified. However, Stewart (1968) has shown that errors in the thermal parameters have their greatest effects on the static charge density at the atom center. At distances beyond about 0·3 Å, the errors in the static valence charge density become more important. Maps of the e.s.d. in the calculated charge density have been derived from the least-squares e.s.d.'s in the atom positional parameters (neutron values), and pseudoatom radial and population parameters. The e.s.d.'s are summarized in the captions of Figs. 4 and 5.

(d) *Refinements involving the oxygen asphericity shifts*

Variations in the structure model were made in an effort to determine whether the best agreement with the

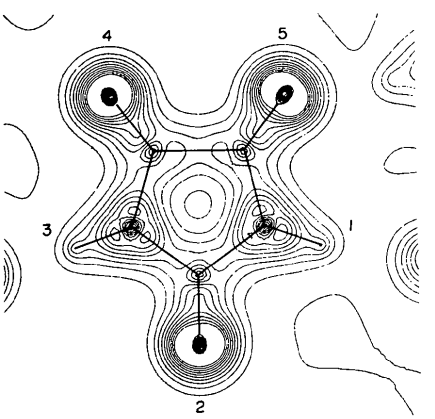

Fig. 5. Total valence-shell charge density for the molecule at rest. Contours are at 0·5 e Å^{-3} and are shown up to 5 e Å^{-3}. The maximum density (7·3 e Å^{-3}) is near O(5). The maximum e.s.d. is 0·20 e Å^{-3} at 0·3 Å from the O centers. It has the value 0·12 e Å^{-3} at the H centers and near the N atoms and 0·07 e Å^{-3} near the C atoms. Since the radial density function is zero at non-hydrogen pseudoatom centers, the valence charge would be zero at these points, except for the contribution from other pseudoatoms. The omitted core density rises sharply to a cusp with large values at the pseudoatom centers (823 e Å^{-3} for C).

data had been obtained. First, the 24 non-hydrogen atom positional parameters were included as variables in the X-ray refinement. Convergence was obtained with $R(F) = 0{\cdot}029$, $R_w(F) = 0{\cdot}017$, QME = 1·23. According to the R-factor ratio test, the additional parameters lead to a highly significant* improvement in the agreement. The atomic parameters from this refinement are also given in Table 2, and the resulting charge-deformation and residual-density maps are shown in Figs. 6 and 7. The changes in C and N positions were less than 0·003 Å. The important differences were for the O atoms [0·010, 0·012, 0·012 Å for O(2), O(4) and O(5) respectively]. These changes give carbonyl bonds which are longer by 0·007, 0·011, 0·007 Å (e.s.d., 0·002 Å) and also give bigger displacements (−0·005, 0·003, −0·006 Å) from the best least-squares molecular plane (Table 3).

The O atom shifts are similar in magnitude and direction to the so-called asphericity shifts noted in other crystal structures which have been determined by both neutron and X-ray diffraction (Coppens, 1974). They can be supposed to arise when spherically symmetric X-ray scattering factors are used to describe an electronic charge distribution for an atom which is actually aspherical because of a dipole deformation. The population parameters (Table 2*d*) show that there are significant dipole deformations at all three O atoms in both refinements. The failure of the dipole deformations to compensate for the asphericity shift comes from the restriction that a common radial parameter was assumed for all O multipole terms. Its value ($\alpha =$ 4·3 a.u.) is largely determined by the O valence-shell monopole term. To be effective in the region closer to the nucleus the radial function for a pseudoatom dipole deformation would need to have a larger α value (Fig. 8).

The difference Fourier map (Fig. 4*b*) near the atom center O(4) has possibly significant features which resemble a residual dipole deformation. It was considered that these might arise from a charge deformation which is quite close to the atom nucleus but which appears to be further away because of thermal vibrational averaging and Fourier-series termination effects. When the difference map was recalculated including only reflections with $\sin\theta/\lambda > 0{\cdot}7$ Å^{-1}, the residual dipole feature was unchanged. The dipole radial scattering factor, f_d, with $\alpha = 4{\cdot}35$ a.u. has little effect on reflections with $\sin\theta/\lambda > 0{\cdot}7$ Å^{-1} (Fig. 8*a*). It was concluded that the asphericity shift comes from a deformation of the inner or core density region of the O pseudoatom, or, in reciprocal space, from reflections with high $\sin\theta/\lambda$. In other crystal structures, the asphericity effect has been attributed to the scattering from O lone-pair density at high $\sin\theta/\lambda$ (Wang, Blessing, Ross & Coppens, 1976).

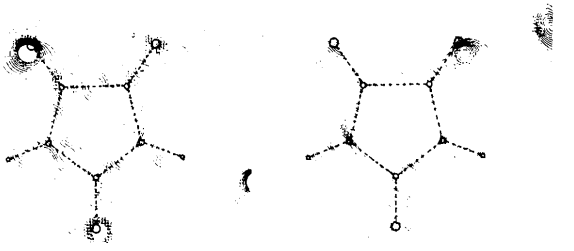

(*a*) (*b*)

Fig. 7. The map of deformations in the charge density in sections above and below the plane of the molecule. These maps correspond to Fig. 6(*a*). (*a*) The section 0·4 Å below the molecular plane. (*b*) The section 0·4 Å above the molecular plane.

* The significance test used throughout for the R-factor ratio is at the confidence level of 99·9%.

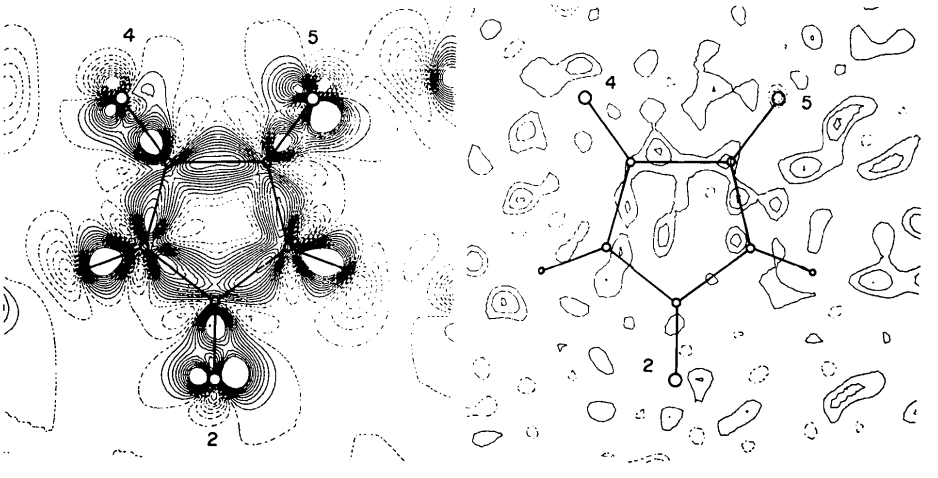

(*a*) (*b*)

Fig. 6. Maps for the X-ray refinement with X-ray values for the non-hydrogen positions. The maps are analogous to those in Fig. 4. (*a*) The map of deformations in the valence charge for the molecule at rest. (*b*) Difference Fourier synthesis showing the residual charge density.

In the case of parabanic acid, two possible explanations were considered. A core deformation could arise from the averaging of curvilinear thermal vibrations such as molecular librations (Willis & Pryor, 1975). If the core electron density follows the nuclear motion exactly, then the thermal-motion parameters c_{jkl} as determined from the neutron data (see above), should also apply to the motion of the cores. An X-ray refinement was carried out using fixed positional and c_{jkl} thermal parameters with values determined from the neutron data. Convergence was obtained with $R(F) = 0{\cdot}020$, $R_w(F) = 0{\cdot}030$ and QME = 1·41, representing a deterioration in agreement. When all but the 18 most significant c_{jkl} values were set to zero, the refinement converged without this deterioration. However, the revised model gave no improvement in agreement and the resulting charge-deformation map showed distortions from the approximate molecular symmetry which appeared to lack physical significance. The failure of the inclusion of neutron c_{jkl} values to improve the X-ray refinement was disappointing in view of the similarities already noted between Figs. 3 and 4(*b*).

Table 3. *Best molecular least-squares plane*

The equation of the plane with respect to the crystallographic axes is

$$1{\cdot}1741x + 6{\cdot}6594y + 2{\cdot}8605z = 3{\cdot}7377$$

where the coefficients are in Å and x,y,z are fractional atomic coordinates from the neutron data. The e.s.d.'s in atomic distances from the plane are 0·001 Å for C, N, O and 0·002 Å for H.

Distances of atoms from the plane (Å)

N(1)	0·004	O(4)	0·001
C(2)	0·002	C(5)	−0·002
O(2)	−0·003	O(5)	−0·001
N(3)	0·001	H(1)	−0·002
C(4)	−0·002	H(3)	−0·002

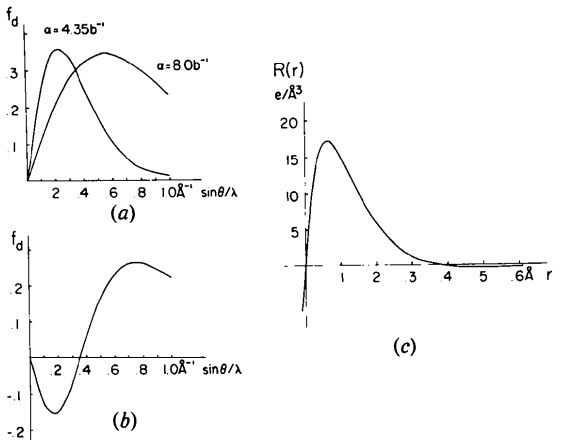

Fig. 8. Dipole radial scattering factors, $f_d(\sin\theta/\lambda)$, and the radial charge density, $R(r)$. (*a*) Scattering factors for dipoles which are sharp (f_S; $\alpha = 8{\cdot}0$ a.u. or bohr^{-1}) and diffuse (f_D; $\bar{\alpha} = 4{\cdot}35$ a.u.) in density space. (*b*) The combined dipole scattering factor, $f_S - 0{\cdot}8f_D$. (*c*) The charge density corresponding to (*b*).

Core polarizations in the charge density for the molecule at rest (Bentley & Stewart, 1974) could provide a second explanation for the O atom asphericity shifts. An X-ray refinement was carried out including a second independent dipole deformation at each O atom. An initial large value of $\alpha = 15$ a.u. was chosen for the radial scattering factor so that the deformation would affect the core region. The atom positional parameters were fixed at the values obtained from the conventional neutron refinement (Table 2*a*). Convergence was obtained with $R(F) = 0{\cdot}030$, $R_w(F) = 0{\cdot}018$ and QME = 1·27. The R factor ratio test indicated that the additional dipole parameters gave a significantly improved model. However, the agreement was not as good as in the X-ray refinement with the non-hydrogen atom positional parameters as variables.

The final dipole parameters from this refinement are in Table 2(*e*). The sharp dipole deformations ($\alpha = 8$ a.u.) had maximum positive values in the direction corresponding to the asphericity shift, *i.e.* on the side of the O opposite to the bonded C atoms. It was noted that the sharp ($\alpha = 8$ a.u.) and diffuse ($\alpha = 4{\cdot}35$ a.u.) dipole deformations at each O atom were antiparallel within experimental error. Thus, unit vectors parallel to the sharp and diffuse deformations happened to make the same angle (169°) at each O atom, and the sum of these unit vectors was 0·19, 0·19, 0·20 at O(2), O(4) and O(5) respectively, none being significantly different from zero in terms of its e.s.d. (0·30, 0·18, 0·22). The diffuse deformation enhances the valence charge in the O—C bonding region, while the sharp deformation has the opposite sense. In reciprocal space, a dipole radial scattering factor for oxygen, $f_d = f_S - 0{\cdot}8f_D$, could be used to approximate the combined deformations, where subscripts D and S refer to the curves in Fig. 8 with $\alpha = 4{\cdot}35$, 8 a.u., respectively. The weighting factor (0·8) comes from the relative population parameters (Table 2*e*). The resultant f_d at low $\sin\theta/\lambda$ resembles the calculated dipole scattering factor for O in carbon monoxide ($^3\pi$), which was derived from the Hartree–Fock charge density (Bentley & Stewart, 1975). The comparison is of interest because of the presumed resemblance in electronic structure between carbon monoxide in this excited state and a carbonyl group. However, the f_d curves differ increasingly with $\sin\theta/\lambda$. The curve for CO($^3\pi$) has a second nodal point near $\sin\theta/\lambda = 1{\cdot}0$ Å^{-1}, where the experimental curve is significantly positive. It is doubtful that the sharp dipoles are exclusively a property of the static charge-density distribution.*

An effort was made to refine the sharp dipole parameters with the inclusion of the 18 most significant c_{jkl} thermal parameters fixed at the neutron values. This

* In a theoretical study of the charge density in diatomic molecules, Epstein & Stewart (1979) show that the neglect of anharmonic thermal motion for non-hydrogen pseudoatoms produces apparent sharp dipoles.

refinement gave the lowest residual of any obtained (QME = 1·22), but in other respects was considered to be unsatisfactory. The sharp dipole radial parameter increased (14 a.u.) but with an e.s.d. (7 a.u.) so large that the value became almost meaningless. Values of the dipole population parameters failed to converge. Also the charge deformation map retained non-symmetrical features similar to those noted after the previous refinement which included c_{jkl} parameters.

(e) *Summary of the refinements*

It is believed that the model which incorporates both the polarization of the static core density, and third-order temperature factors would be the most appropriate. However, it appears that more accurate c_{jkl} values are needed. In the case of parabanic acid, the effect of the substantial errors in the neutron c_{jkl} values would be further amplified for the X-ray reflections which have sin θ/λ greater than the maximum for the neutron data (0·76 Å^{-1}). No effort was made to carry out an X-ray refinement of the c_{jkl} parameters together with the sharp dipole parameters, because very strong parameter correlations would be expected. The correlations might diminish if the X-ray intensity data were to extend to sin θ/λ values greater than about 1·3 Å^{-1}, where the radial scattering factor f_d for $\alpha = 8$ a.u. becomes negligible (Fig. 8*a*). However, low temperatures would be needed for such measurements.

Because the nature of the core-density deformations is poorly defined in terms of the available X-ray and neutron intensity data, further discussion is based on the two X-ray refinements which involved spherical core-scattering factors. The best choice for each non-hydrogen pseudoatom center probably lies in the range between the neutron and X-ray positions (Table 2*a*). There is a corresponding uncertainty in the valence charge density, which is most noticeable as differences in the O dipole population parameters (Table 2*d*) and in the regions about the O atoms in the deformation density (Figs. 4*a*, 6*a*). Similar differences in deformation density occur in the sections parallel to the molecular plane, although only the maps based on the X-ray positional parameters are shown (Fig. 7). Thus the effect of the asphericity shift is to produce differences in the deformation maps (Figs. 4*a*, 6*a*) which are analogous to the differences between *X*–*X* and *X*–*N* maps, *e.g.* in the crystal structure of *p*-nitropyridine *N*-oxide (Wang, Blessing, Ross & Coppens, 1976).

Discussion

(a) *The nuclear configuration*

In the crystal structure of parabanic acid, the molecule is planar (Table 3) within twice the uncertainty in the neutron positional parameters. In the crystal complex with 9-ethyladeninium oxalurate (Shieh & Voet, 1975) the parabanic acid molecule shows a slight twist with respect to an axis through C(2) and the midpoint of the C(4)–C(5) bond, so that the carbonyl O(4) and O(5) atoms are displaced 0·03 Å on opposite sides of the best least-squares plane.

The neutron bond lengths and angles are given in Fig. 1 before and after a correction for rigid-body libration of the molecule. As shown in Table 4, the neutron thermal parameters agree satisfactorily with rigid-body behavior (Schomaker & Trueblood, 1968), particularly when the H atoms are omitted. The uncorrected neutron bond lengths and angles agree within experimental error with the X-ray values of Davies & Blum (1955) and Shieh & Voet (1975). There is also agreement with values for parabanic acid in the complex with urea when the calculations are carried out using the atomic coordinates of Colman & Medlin (1970) and the unit-cell parameters recently redetermined by Ruble (1978).

The C(4)–C(5) bond is long (1·539 Å, or 1·551 Å after correction) which suggests that it has very little double-bond character. Other long C–C bonds occur in oxalic acid (1·539 Å; Coppens & Sabine, 1969) and oxamide (1·534 Å; de With & Harkema, 1977) which also have coplanar vicinal carbonyl groups, although in these cases the carbonyl bonds are *trans*, rather than *cis* as in parabanic acid.

Table 4. *Rigid-body analysis for parabanic acid*

Calculations were based on non-hydrogen atom neutron U_{ij} values transformed to the crystal axes *a*, *b*, *c**.

Translational tensor Units: Å × 10⁴			Librational tensor Units: deg²			Cross tensor Units: Å deg × 10²		
153 (4)	7 (3)	4 (3)	10·5 (6)	3·9 (5)	−0·9 (5)	2 (2)	−2 (1)	6 (1)
	220 (5)	−2 (4)		22·9 (10)	−13·1 (10)	−6 (1)	−11 (2)	8 (1)
		214 (4)			24·6 (15)	−9 (2)	7 (1)	9

The principle values of the librational tensor are 37·4, 12·6 and 8·2 deg².
The r.m.s. difference between observed and calculated U_{ij} values is 0·0006 Å².

It is of interest to compare bond lengths and angles for the planar –CO–NH–CO–NH–CO– system with those in 5,5-diethylbarbituric acid (barbital) which were recently determined for polymorph II at 198 K by neutron diffraction (McMullan, Fox & Craven, 1978). In parabanic acid, the end C atoms of this system bond with each other, whereas in barbital they are bonded through an intervening tetrahedral C atom to form a planar six-membered ring. The average internal ring angle must be smaller by 12° in parabanic acid. However, the observed angle changes are non-uniform, with the greatest change (14·7°) at the N atoms, and significant differences in the changes at the carbonyl C atoms, which are 9·0° at C(2) and 13·9° at C(4). The C(2)–N(3) and C(4)–N(3) bond lengths at the same nitrogen have thermally corrected neutron values of 1·396, 1·360 Å in parabanic acid and 1·389, 1·372 Å in barbital. The smaller difference (0·017 *vs* 0·036 Å) in barbital was unexpected, since it indicates that the presence of a tetrahedral C atom in the ring leads to a greater degree of conjugation in the C–N bonds.

In the crystal structure of parabanic acid, there is nothing unusual in the geometry of the two hydrogen bonds, N(1)H(1)···O(4) and N(3)H(3)···O(5). The N···O distances are 2·88, 2·85 Å with H···O distances 1·89, 1·82 Å and N–H···O angles 163, 171° respectively.* The short intermolecular C···O distances (Fig. 2) are not significantly different from those of Davies & Blum (1955).

(*b*) *The charge density*

In the multipole representation of the pseudoatom charge density, only the monopole term contributes to the net valence charge. Each higher multipole term is a deformation from spherical symmetry with regions of electronic charge enrichment (positive) and depletion (negative), which sum over all space to give a net zero charge, irrespective of the corresponding population parameter.

In parabanic acid, the monopole population parameters (p_v, Table 2*d*) have values which are not significantly different from those of electrically neutral pseudoatoms. However, these populations and the associated radial density parameters (α) must be interpreted with caution because of their strong correlations and their sensitivity to the assumed structural model. Thus, in the least-squares refinement which included both sharp and diffuse dipole deformations for the oxygens, the average p_v values were 3·88 (5), 5·14 (7), 6·14 (4) and 0·83 (6) for C, N, O and H respectively. The corresponding α values were 3·28 (2), 3·84 (2), 4·35 (1) and 2·24 (7) a.u. In the different least-squares refinements carried out with unconstrained population parameters, the sum of p_v values was always within a few per cent of the value (42) for a neutral molecule.

The values obtained for the radial parameters, except possibly for N, are less than the standard values of 3·44, 3·90, 4·50, 2·48 a.u. for C, N, O and H which are based on molecular-orbital calculations (Hehre, Stewart & Pople, 1969). Thus, the charge densities for parabanic acid pseudoatoms tend to be more diffuse than is predicted from consideration of the energy of an isolated molecule.

In parabanic acid, the p_v and α values are similar to those found in 1,1′-azobiscarbamide and 2,4,6-triamino-*s*-triazine (Cromer, Larson & Stewart, 1976). These are the other two organic crystal structures which have been refined by Stewart's (1976) pseudoatom procedure at the octapole level.

A consideration of the higher multipole population parameters (Table 2*d*) and the corresponding charge deformation maps (Figs. 4*a*, 6*a*, 7) shows that the nature of the charge deformation is different for each type of pseudoatom (C,N,O,H). At both H atoms the deformation density is dominated by the dipole terms, which contribute density in the NH bond at the expense of the H···O hydrogen-bonding region. At the N atoms, the largest deformations come from the octapole terms which enhance the density in the three bonds at the expense of the region between the bonds. The C atoms have important quadrupole as well as octapole terms. The C octapoles have a similar effect to those of N while the C quadrupole depletes charge from the region above and below the molecular plane (Fig. 7). Although there are differences in the deformations at the three O atoms, they also have features in common. At each O, the quadrupole deformation is strongest, with negative regions along the C–O bond and positive regions of nonbonding density in directions perpendicular to the C–O bond. The latter have maximum values of 1·00, 0·45, 1·01 e Å^{-3} at O(2), O(4) and O(5) respectively. The quadrupole deformation at O(4) differs from the others both in magnitude, and with respect to rotation about the C–O bond. A line through the O center and the positive quadrupole maxima is rotated from the molecular plane by angles 5, 45 and 11° respectively.* The unequal positive charge density in the two nonbonding regions at each O comes primarily from weaker octapole deformations with maximum magnitudes ranging from 0·2 to 0·3 e Å^{-3}. The combined quadrupole and octapole deformations at the O atoms are similar in the structure refinements which use neutron or X-ray data to determine the O

* Intermolecular distances and angles here and in Fig. 2 are not corrected for thermal-motion effects. The values are given with less precision than is indicated from the least-squares e.s.d.'s (0·002 Å and 0·2°).

* Carbonyl O atom nonbonded density located above and below the amide plane has also been observed in acetamide in the crystal complex with allenedicarboxylic acid (Berkovitch-Yellin, Leiserowitz & Nader, 1977), in formamide (Stevens, 1978) and in polymorph II of barbital (Fox, Weber & Craven, 1979). Further discussion of this effect is deferred.

centers. In these two refinements, the greatest differences come from the O dipole deformations, which are directed approximately along the C–O bonds but have opposite senses. With the X-ray-determined O positions, the dipole deformations are positive in the C–O bonding region.

In considering the charge density in the bonding regions, the overlap of pseudoatom deformation densities is of greater interest, although the contribution from the overlap of spherical or monopole density has greater magnitude. Thus, at the center of the C(4)–C(5) bond (Fig. 5), the combined deformations give a density 0·4 e Å^{-3}, while the monopole terms contribute 1·3 e Å^{-3}. Within bonds of the same type (N–H, C–O, C–N) the bonding densities are similar, including the two C–N bonds at each N, which differ by at least 0·03 Å in length. In every bond, the maximum positive deformation density is close to the line of atom centers. The C–N and C–O bonds appear to have polar character. Thus, in the planes 0·4 Å above and below the ring (Fig. 7) where π-bonding density might occur, there is depletion at the C atoms with enrichment about the N atoms. In each C–O bond, the σ-bonding region shows a strong contribution of positive density from only the C. Overlap of positive deformation density occurs as a bridging between this region near the C and the quadrupole maxima near the O.

A map of charge-density deformations for formamide has been calculated by *ab initio* self-consistent field methods (Fig. 2 in Stevens, Rys & Coppens, 1978). The theoretical map agrees very well with the experimental maps for the parabanic acid fragments CO–NH involving O(2) and O(5), particularly those in Fig. 4(*a*) in which the atom centers were determined from the neutron data. In the following comparison, peak deformation densities (e Å^{-3}) of the fragment O(5)–C(5)–N(1)–H(1) in Fig. 4(*a*) are given, together with the corresponding formamide values (in parentheses) estimated from the theoretical map. Maximum densities in the O atom nonbonding region are +1·0 and +1·1 (1·0). Along the C–O bond, the peak densities are −1·0 (−0·9) and +0·9 (0·6). In the C–N and N–H bonds, the densities are +0·6 (0·5) and +0·8 (0·7). The quality of this agreement supports the assumption that the valence-shell charge density has been deconvoluted from the thermal motion.

In parabanic acid, an inspection reveals no simple relationship between the observed deformation density and hydrogen-bond formation, except that the interaction would be promoted by the dipole deformation at each H atom, which deshields the proton from the O acceptor atom. At the acceptor O(4) and O(5) atoms there is a tendency for greater nonbonding density to occur on the side nearer to the NH donor group (Figs. 6*a*, 7), but there is no well-defined polarization of O charge close to the line of centers O···H. It would appear that directional character in the hydrogen bond comes primarily from the N–H donor.

Likewise, the short internuclear C···O distances in parabanic acid (Fig. 2) appear to have little effect on the valence charge density. Thus, the deformation density is symmetric with respect to the ring plane near all three C atoms (Fig. 7). The charge depletion in these regions suggests that the van der Waals radius for C in a carbonyl group could be reduced so that some smaller intermolecular C···O distance (2·8 Å) becomes normal. However, it should be recognized that deformations of the O core densities may also be involved. These deformations give rise to the O asphericity shifts whereby, according to the X-ray atomic positions, the molecule becomes non-planar. In the X-ray refinement in which the asphericity shifts were treated as dipole deformations of the O core density (Table 2*e*), the positive ends of the dipoles at each O atom were found to be directed towards the voids between neighboring molecules. In Fig. 2, the O(2) sharp dipole on the central molecule is directed across the page towards the center of the quadrilateral of C atoms which are at short C···O distances and, also, the dipole on O(5) is directed towards the nearest C(2). Although the directions of the O asphericity shifts can be related to the arrangement of the molecules in the crystal structure, it remains to be determined whether the effect arises from the thermal motion, from an electrostatic interaction, or from both.

The neutron structure determination was carried out at Brookhaven National Laboratory under contract with the US Department of Energy and supported by its Division of Basic Energy Sciences. We thank Mr Joseph Henriques for technical assistance in the neutron data collection. The X-ray structure determination was supported by Grant GM-22548 from the National Institutes of Health. We are grateful for discussions of the X-ray work with Drs Robert F. Stewart and Joel Epstein of Carnegie–Mellon University and Dr Peter Trucano of the University of Pittsburgh. We thank Drs R. Shiono and Hans-Peter Weber for computing assistance.

References

ANDREWS, J. C. & SELL, I. T. (1955). *Arch. Biochem. Biophys.* **56**, 405–411.

BATS, J. W., COPPENS, P. & KOETZLE, T. F. (1977). *Acta Cryst.* B**33**, 37–45.

BECKER, P. J. & COPPENS, P. (1974). *Acta Cryst.* A**30**, 129–147.

BENTLEY, J. & STEWART, R. F. (1974). *Acta Cryst.* A**30**, 60–67.

BENTLEY, J. & STEWART, R. F. (1975). *J. Chem. Phys.* **63**, 3794–3803.

BERKOVITCH-YELLIN, Z., LEISEROWITZ, L. & NADER, F. (1977). *Acta Cryst.* B**33**, 3670–3677.

BOLTON, W. (1964). *Nature (London)*, **201**, 987–989.

BÜRGI, H. B., DUNITZ, J. D. & SHEFTER, E. (1974). *Acta Cryst.* B**30**, 1517–1527.
CLEMENTI, E. (1965). *IBM J. Res. Dev.* Supplement, **9**, 2.
COLMAN, P. M. & MEDLIN, E. H. (1970). *Acta Cryst.* B**26**, 1547–1553.
COPPENS, P. (1974). *Acta Cryst.* B**30**, 255–261.
COPPENS, P. & HAMILTON, W. C. (1970). *Acta Cryst.* A**26**, 71–83.
COPPENS, P. & SABINE, T. M. (1969). *Acta Cryst.* B**25**, 2442–2451.
COPPENS, P. & STEVENS, E. D. (1977). *Isr. J. Chem.* **16**, 175–179.
CRAVEN, B. M. & WEBER, H.-P. (1977). *The 'POP' Least-Squares Refinement Procedure*, Tech. Rep., Department of Crystallography, Univ. of Pittsburgh.
CROMER, D. T., LARSON, A. C. & STEWART, R. F. (1976). *J. Chem. Phys.* **65**, 336–349.
DAVIES, D. R. & BLUM, J. J. (1955). *Acta Cryst.* **8**, 129–136.
EPSTEIN, J. & STEWART, R. F. (1977). *J. Chem. Phys.* **66**, 4057–4064.
EPSTEIN, J. & STEWART, R. F. (1979). *Acta Cryst.* A**35**. In the press.
FOX, R. O. JR, WEBER, H.-P. & CRAVEN, B. M. (1979). In preparation.
GARTLAND, G. L. & CRAVEN, B. M. (1974). *Acta Cryst.* B**30**, 980–987.
HAMILTON, W. C. (1974). *International Tables for X-ray Crystallography*, Vol. IV, pp. 285–310. Birmingham: Kynoch Press.
HAMILTON, W. C., ROLLETT, J. S. & SPARKS, R. A. (1965). *Acta Cryst.* **18**, 129–130.
HEHRE, W. J., STEWART, R. F. & POPLE, J. A. (1969). *J. Chem. Phys.* **51**, 2657–2664.
HIRSHFELD, F. L. (1977). *Isr. J. Chem.* **16**, 168–174.
JOHNSON, C. K. (1970). *Thermal Neutron Diffraction*, edited by B. T. M. WILLIS, pp. 132–160. Fairlawn, New Jersey: Oxford Univ. Press.
JOHNSON, C. K. & LEVY, H. A. (1974). *International Tables for X-ray Crystallography*, Vol. IV, pp. 311–336. Birmingham: Kynoch Press.
MCMULLAN, R. K., FOX, R. O. JR & CRAVEN, B. M. (1978). *Acta Cryst.* B**34**, 3719–3722.
RUBLE, J. (1978). Private communication.
SCHOMAKER, V. & TRUEBLOOD, K. N. (1968). *Acta Cryst.* B**24**, 63–76.
SHIEH, H. S. & VOET, D. (1975). *Acta Cryst.* B**31**, 2192–2201.
STEVENS, E. D. (1978). *Acta Cryst.* B**34**, 544–551.
STEVENS, E. D., RYS, J. & COPPENS, P. (1978). *J. Am. Chem. Soc.* **100**, 2324–2328.
STEWART, R. F. (1968). *Acta Cryst.* A**24**, 497–505.
STEWART, R. F. (1976). *Acta Cryst.* A**32**, 565–574.
TAKUSAGAWA, F. & KOETZLE, T. F. (1979). *Acta Cryst.* B**35**, 867–877.
VARGHESE, J. N., O'CONNELL, A. M. & MASLEN, E. N. (1977). *Acta Cryst.* B**33**, 2102–2108.
VOET, D. (1972). *J. Am. Chem. Soc.* **94**, 8213–8222.
WANG, Y., BLESSING, R. H., ROSS, F. K. & COPPENS, P. (1976). *Acta Cryst.* B**32**, 572–578.
WILLIS, B. T. M. & PRYOR, A. W. (1975). *Thermal Vibrations in Crystallography*. Cambridge Univ. Press.
WITH, G. DE & HARKEMA, S. (1977). *Acta Cryst.* B**33**, 2367–2372.

Acta Cryst. (1979). B**35**, 945–948

2-*O*,3-Diethyl-7,8,10-trimethylisoalloxazinium Perchlorate

BY MARIANNE VON GLEHN

Department of Structural Chemistry, Arrhenius Laboratory, University of Stockholm, S-106 91, *Sweden*

AND ROLF NORRESTAM*

Structural Chemistry Group, Chemistry Department B, The Technical University of Denmark, DK-2800 *Lyngby, Denmark*

(*Received* 15 *September* 1978; *accepted* 9 *January* 1979)

Abstract

The crystal structure of 2-*O*,3-diethyl-7,8,10-trimethylisoalloxazinium perchlorate, $C_{17}H_{21}N_4O_2^+.ClO_4^-$, has been determined from X-ray diffraction data collected at room temperature. The structure is monoclinic, space group $P2_1/c$, with $a = 10{\cdot}73$ (1), $b = 12{\cdot}91$ (1), $c = 16{\cdot}52$ (1) Å, $\beta = 122{\cdot}18$ (5)°, $V = 1936{\cdot}9$ Å^3, $Z = 4$ and $D_x = 1{\cdot}42$ Mg m^{-3}. The derived structural model was refined to a conventional linear R value of 0·056. The structural results confirm the assumed planarity of the alloxazinium ring system of the molecule. The perchlorate ions are located above the central region of the ring system in such a way that discrete alloxazinium perchlorate entities are formed. The perchlorate ions are disordered in a way corresponding to two different orientations of the ions at the same crystallographic site.

* To whom correspondence should be addressed.

0567-7408/79/040945-04$01.00